The effects of laser peening on laser additive manufactured 316L steel

Yi Lu[1,2] · G. F. Sun[1] · Z. D. Wang[1] · B. Y. Su[1] · Y. K. Zhang[1,3] · Z. H. Ni[1]

Abstract

Laser peening has an extensive application in traditional manufacturing industry. However, in additive manufacturing, the initial stresses on the parts often reduce the effects of laser peening and make it hard to achieve a desirable residual stress distribution. In this investigation, the interaction of initial residual stress and laser peening-induced stress was studied through numerical simulation and experimental tests. A finite element model (FEM) model was built to predict the stress distribution on laser-deposited sample, and its changed state is affected by laser peening. The microstructure and mechanical properties were also characterized experimentally. The result turned out that the thermal-induced tensile residual stress in laser-deposited sample can affect the laser peening result in both horizontal and longitudinal directions. Some mechanical properties of the LAMed sample were changed after LSP treatment. The hardness on the surface and 1-mm depth have been increased by 7% and 22%, respectively, and the yield strength was increased by 16%, while there is no significant change in the tensile strength and elongation rate.

Keywords Laser peening · Laser additive manufacturing · Finite element analysis · Residual stress

1 Introduction

Like an inkjet printer, the products produced through laser additive manufacturing (LAM) are formed by laser-melted metal from point to point in a three-dimensional space [1]. The heating, melting, and solidification happen in every step of the additive manufacturing process. The repeated heating and cooling create spatially varied thermal cycles which induce a complex residual stress field in components. The residual stress affects the surface hardness, tensile strength, corrosion resistance, and fracture toughness of the component and can even cause cracking and distortion when it exceeds the yield strength of the material. To impart improved properties into LAMed products, the residual stress should be regulated to fulfill various working conditions. The residual stress state of the LAMed components can be adjusted by optimizing laser parameters, scan strategy, powder ingredient, preheating [2–5],.etc. These methods can effectively prevent cracking and distortion defects; however, it is hard to adjust the stress in some critical points.

There are several ways to adjust surface stress distribution, such as surface polishing, rolling, shot peening, ultrasonic peening, and laser shock peening [6–9]. Among these methods, laser shock peening (LSP) is the most suitable surface strengthening technology for LAM [10]. First, the LSP has the best geometric adaptability. The characteristic of LAM is to build the parts which are hard or impossible to produce by conventional subtractive machining, and the geometric features of the LAM parts are usually nonuniform and complex. The conventional stress-relieving strategy such as surface polishing and rolling is hard to reach some corners and dents on the sample [11]. Second, compared with the shot peening and ultrasonic peening, LSP creates less surface strain and shape change, which can be applied to some thinner and minute structure on the products [12]. Third, LSP is superior in improving fatigue and anti-corrosion performance. LAM technology is widely applied in the aerospace and biomedical

✉ G. F. Sun
  gfsun@seu.edu.cn

✉ Z. H. Ni
  nzh2003@seu.edu.cn

1 School of Mechanical Engineering, Southeast University, Nanjing, Jiangsu 210096, People's Republic of China

2 School of Mechanical and Electrical Engineering, Wenzhou University, Wenzhou, Zhejiang 325035, People's Republic of China

3 School of Mechanical and Electrical Engineering, Guangdong University of Technology, Guangzhou, Guangdong 510006, People's Republic of China

industry which has a high demand for long fatigue life and good corrosion resistance performance.

Beneficial residual stress and microstructure refinement are the most concerned feature induced by LSP process. Many studies have concentrated on this part. In additive manufacturing, Hackel [12] compared the effect of shot peening and LSP on additive manufactured parts; they pointed out that laser peening would be especially beneficial for applications where geometry requirements create areas of increased stress such as in fillets and notched areas leading to local stress risers. Hurtado [13] studied the effectiveness of LSP on the residual stress mitigation of laser-cladded S275 and 316 steel. They found that tensile residual stresses were generated on the laser-cladded surface in both longitudinal and transverse directions, and LSP can introduce significant levels of compressive stress (~ 200–300 Mpa) to the overlays. Guo [14] studied LSP effect on additive manufactured Ti6Al4V titanium alloy. The results turned out that the LSP can create compressive residual stress with the maximum value of around 200 MPa, and an affected depth of 700 μm and the microstructure in the surface layer were refined after peening. Sun [15] applied the LSP technology on additive manufactured 2319 aluminum alloy; they found that LSP can refine the surface microstructure and enhance the microhardness and tensile properties. Shiva [16] compared the effects of laser annealing and laser shock peening on additive manufactured Ni–Ti memory alloy; they got the same conclusion that the LSP can induce compressive residual stress to prevent the surface crack formation. They also built a simple FEM model to estimate the residual stress of the laser-peened sample, but they did not consider the initial stress in the as received sample. Kalentics [17] integrated laser peening into laser additive manufacturing. During the manufacturing, the LSP was conducted on each laser-deposited layer. The results turned out that the integrated LSP successfully induces compressive residual stress into the additive manufactured layer, but the parameter cooperation between LSP and laser-deposited layer thickness needs to be further optimized to achieve the desired residual stress contour for a given application. Although it has been approved that the LSP technology is a promising tool to enhance additive manufactured parts, the residual stress superstition mechanism caused by LSP is still not fully understood. Furthermore, the uncontrollable superposition of the stress and strain may lead to undesirable deformation and stress distribution. For different applications, it is necessary to predict the LSP-induced residual stress field under a given initial residual stress condition.

The objective of this work is to predict the LSP-induced residual stress superposition on additive manufactured parts and evaluate its effects on microstructural features and mechanical characteristics. A FEM model was developed and verified with experiments to predict the residual stress distribution before and after LSP. The residual stress, microstructure, hardness, and tensile strength were investigated by X-ray diffraction measurements (XRD), optical and scanning electron microscopy (OM, SEM), microhardness tester, and electronic universal testing machine. The effects of the LSP on the residual stress and mechanical characteristics of the additive manufactured material were then discussed in detail.

2 Materials and methods

2.1 Laser deposition

The laser deposition was performed in Southeast University, Nanjing, China, with TruDiode 3006 laser. The laser power applied in the experiment was 800 W, with 2-mm laser diameter. The scan speed was 600 mm/min. The powder used in this article is 1236F/FE-271(Praxair USA), and its composition is close to that of AISI 316 L stainless steel (Table 1). For different analysis purposes, two kinds of samples were printed. To analyze the residual stress distribution, the sample is deposited as the size of 20 mm × 30 mm × 3 mm (Fig 1a, b) with three layers. For the tensile stress test, the sample was printed as the size of 70 mm × 12 mm × 3 mm (3 layers) and then cut with electric discharge machining to dog bone shape (Fig. 1c). The size of the tensile stress sample is shown in Fig. 1 c.

2.2 Laser peening

LSP experiment was carried out on laser-deposited sample by a Q-switched Nd: YAG laser system. The treated areas are plotted in Fig. 1 b and c. The laser machine was operated at 1 Hz repetition rate, 1064 nm wavelength, and 20 ns pulse width. In this work, 3-mm diameter spot size and 50% overlapping rate were used. Pulse energy selected in this experiment was 7 J, and the energy density was calculated as approximately 4.95 GW/cm^2. Before LSP, samples were covered by aluminum foil adhesive coating with a thickness of 0.15 mm to prevent the thermal effects. Additionally, a deionized water film with a thickness of 1–2 mm was used as the transparent confining layer. During LSP, a zigzag scan vector was employed as scanning strategy.

Table 1   Chemical composition of 1236F/FE-271 Praxair power (Wt%)

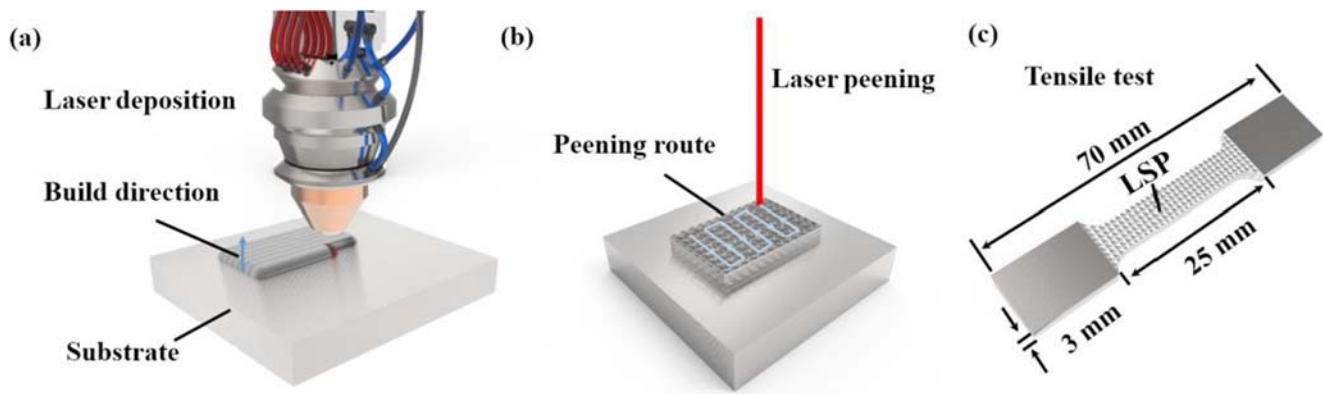| C	Cr	Mn	Mo	Ni	P	S	Fe
0.004	17	1	2	12	0.019	0.004	

Fig. 1 Sample size, **a** sample for residual stress and microstructure analysis, **b** laser peening route, and **c** sample for tensile test

2.3 Microstructure characterization

The microstructure of laser-deposited samples before and after laser peening was evaluated through OM and SEM. The cross sections for microstructure observation were cut perpendicularly to the treated surface. Transmission electron microscopy (TEM) of laser-peened samples was conducted to analyze detailed changes of the microstructure. Samples were put into mechanical thinning from the untreated side for the topmost surface specimens. For further electrolytic thinning, 3-mm disks were punched. Electrolytic thinning of the punched disks was carried out using twin-jet polisher. The subsurface specimen disk was thinned from both sides until perforation, whereas the jet polishing was employed for purpose of back-forward thinning for the top surface specimen.

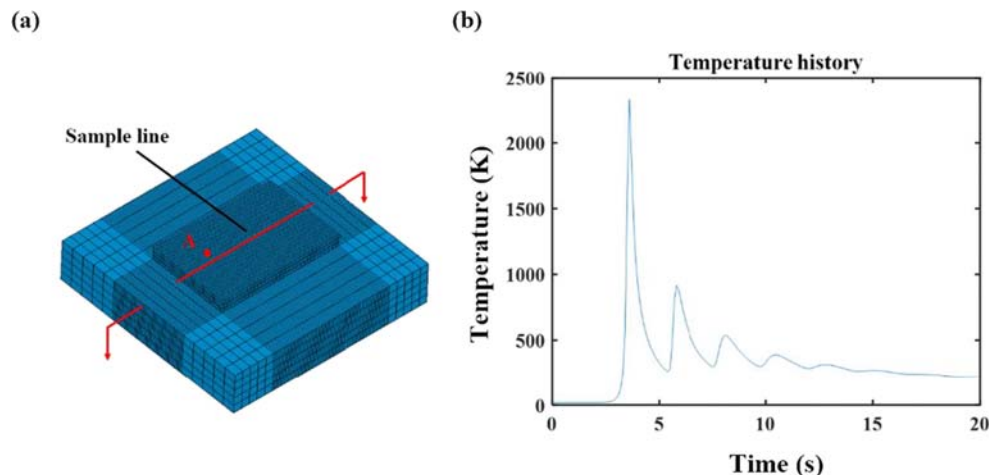## 2.4 Mechanical property test

Microhardness measurements were conducted using HXD-1000TMSC/LCD Vickers hardness test machine. Measurements were made on the polished cross sections going from peened edge to the center of the sample. A load of 200 g was adopted for a dwell time of 10 s and 250 μm was

kept between indents. Each microhardness value was the mean value of two measurements at the same depth.

The residual stresses of laser-deposited samples before and after laser peening were measured by using X-ray diffraction (XRD) with sin2ψ method. The X-ray source was Cr Kα X-ray, and the diffraction plane was (220). The X light tube voltage and current were set at 22.0 kV and 6.0 mA, respectively. Measurements were carried out on each layer of the deposited sample. The stresses on the top layer were measured directly. To measure the residual stress on the middle and bottom layer, the samples were first ground off 0.8 mm thickness material and then polished by electrochemical polishing to remove the residual stress induced by grinding.

The schematic drawing of the tensile test specimens is shown in Fig. 1 c. Before the tensile test, both faces of the gauge area are treated by LSP, as shown in Fig. 1 c. The uniaxial tension test was carried out on a CMT5105 electronic universal testing machine. The test was performed at room temperature with a feed speed of 3 mm/min. The tensile strength and uniform elongation were an average of six testing values to minimize the uncertainties. Fractographic examinations of specimens after completion of tensile tests were carried out using SEM.

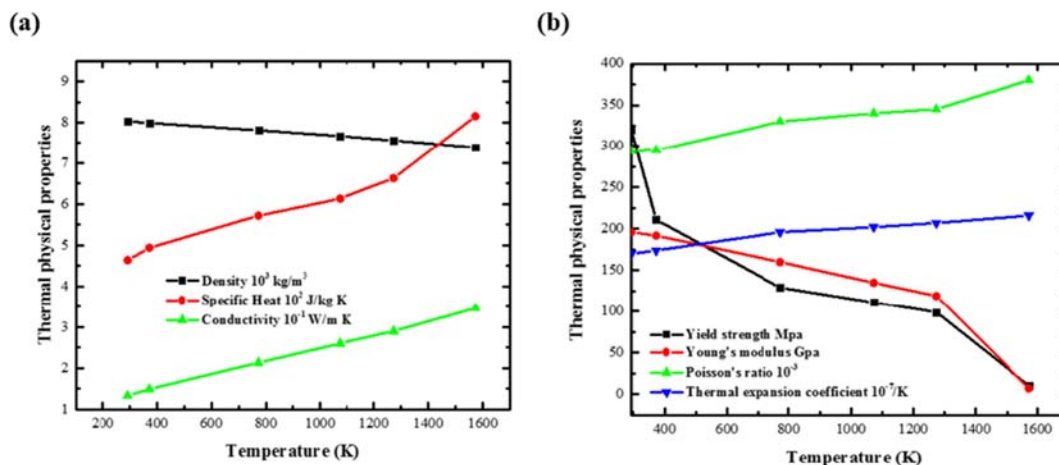Fig. 2 **a** Simulation domain. **b** Temperature history at point A

Fig. 3 Temperature-dependent **a** thermal-physical properties and **b** thermal-mechanical properties of AISI 316 stainless steel

3 Numerical model

The numerical calculation contains three steps. First, a thermal model is built to calculate the full temperature history of laser deposition process. Second, apply thermal-mechanical properties of the material into the model to calculate the stress evolution based on temperature history. Third, take the results from thermal analysis as an initial condition to calculate the laser peening-induced residual stress.

3.1 Thermal analysis

Figure 2 a shows the simulation domain, the deposited cuboid is $30 \times 20 \times 3$ mm, and the substrate is $50 \times 50 \times 10$ mm. The mesh on the deposited part is refined to achieve better calculation accuracy; a total of 24,700 elements are built in the model.

The three-dimensional transient thermal analysis is governed by the equation:

$$\frac{\partial}{\partial x}\left(k\frac{\partial T}{\partial x}\right) + \frac{\partial}{\partial y}\left(k\frac{\partial T}{\partial y}\right) + \frac{\partial}{\partial z}\left(k\frac{\partial T}{\partial z}\right) + Q = \rho c \frac{\partial T}{\partial t} \quad (1)$$

where T represents the temperature, k denotes the thermal conductivity, Q is the laser volumetric heat input, and ρ is the material density. The latent heat of fusion is considered in the model by modified c as [18]:

$$C(T) = C_p(T) + \frac{L}{T_m - T_0} \quad (2)$$

where $C(T)$ is the modified specific heat, C_p is the temperature-dependent specific heat, L is the latent heat of fusion which is set as 365 kJ/kg [19], T_m is the melting temperature, which is set as 1800 C, T_0 is the ambient temperature, temperature and is set as 20 C. The temperature-dependent material properties are drawn in Fig. 3 [20].

The heat source applied in this work is a Gaussian beam; the intensity function can be described as:

$$Q(r) = \frac{2AP}{\pi\omega^2}\exp\left(-\frac{2r^2}{\omega^2}\right) \quad (3)$$

where A is the absorptivity of the steel; in present work, we take $A = 0.4$; P is the laser power; ω is the radius of the beam; and r is the radial distance from the beam center.

To make simulation accurate, the initial and boundary conditions should be defined. The initial temperature is set to 20 °C according to the room temperature. Thermal boundary conditions consider the heat convection in the air, the surface heat radiation to ambient air and conduction. The heat loss can be expressed as:

$$q_{conv} = h_{conv}(T - T_\infty) \quad (5)$$
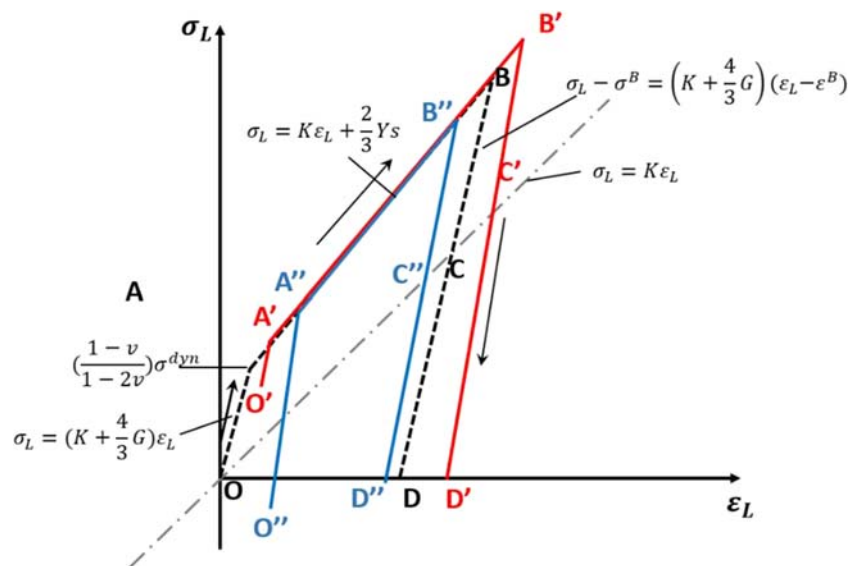
$$q_{rad} = \varepsilon\sigma\left(T^4 - T_\infty^4\right) \quad (6)$$

where h_{conv} is the convective heat transfer coefficient of the shielding gas, ε is the emissivity of the sample, and σ is the Stefan-Boltzmann constant.

For isotropic material, the stress-strain relationship can be written in Cartesian coordinates as follows [21]:

Table 2 Basic material properties for 316 stainless steel

Material properties	Density (Kg·m^{-3})	Poisson ratio v	Elastic modules (GPa)	HEL (GPa)
316 stainless steel	7800	0.29	196	1.47

Fig. 4 The mechanism of laser peening stress superposition

$$\varepsilon_{xx} = \frac{1}{E}\left[\sigma_{xx} \times v(\sigma_{yy} + \sigma_{zz})\right] + \alpha_e \Delta T$$
$$\varepsilon_{yy} = \frac{1}{E}\left[\sigma_{yy} \times v(\sigma_{xx} + \sigma_{zz})\right] + \alpha_e \Delta T \qquad (7)$$
$$\varepsilon_{zz} = \frac{1}{E}\left[\sigma_{zz} \times v(\sigma_{xx} + \sigma_{yy})\right] + \alpha_e \Delta T$$

$$\epsilon_{xy} = \frac{1+v}{E}\sigma_{xy} \quad \epsilon_{xz} = \frac{1+v}{E}\sigma_{xz} \quad \epsilon_{yz} = \frac{1+v}{E}\sigma_{yz} \qquad (8)$$

where E, v, and α_e are the modulus of elasticity, Poisson's ratio, and coefficient of thermal expansion, respectively. ΔT represents a temperature rise at a point (x, y, z) at time t.

3.2 Model of laser peening

To predict the effect of laser peening, the residual stress from the thermal analysis is imported into the explicit calculation model as initial stress. The laser peening can be considered as a confined ablation process. The laser energy passes through a transparent confinement layer (normally water or glass) to ablate the absorption overlay beyond the sample surface. The ablation plasma heated and supported by laser expands

at the sample surface. Constrained by confinement layer, a shock wave was induced and propagated into the sample. In this mode, the peak pressure P is given by:

$$P(GPa) = 0.01\sqrt{\frac{\alpha}{2\alpha + 3}}\sqrt{Z(g\ cm^2 s^{-1})}$$
$$\times \sqrt{I_0(GW\ CM^{-2})} \qquad (9)$$

where P is laser-induced pressure; Z is the reduced shock impedance between sample and confinement layer; and α is the efficiency of the interaction. In water confinement mode, Eq. (9) can be simplified as:

$$P(GPa) = 1.02\sqrt{I_0(GW\ CM^{-2})} \qquad (10)$$

where the pressure pulse is assumed to be uniform over the laser spot.

In the LSP process, strain rates exceed more than $10^6\ s^{-1}$ within the target material. At such a high strain rate, metals behave significantly different from that under quasi-static conditions [22]. In this work, Hugoniot elastic limit (HEL) model
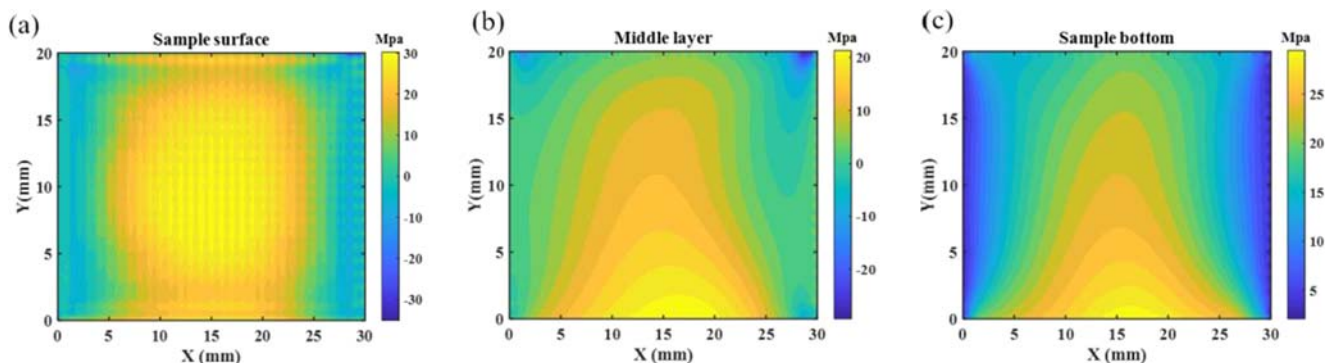

Fig. 5 The residual stress distribution. **a** Sample surface, **b** middle layer, and **c** bottom layer
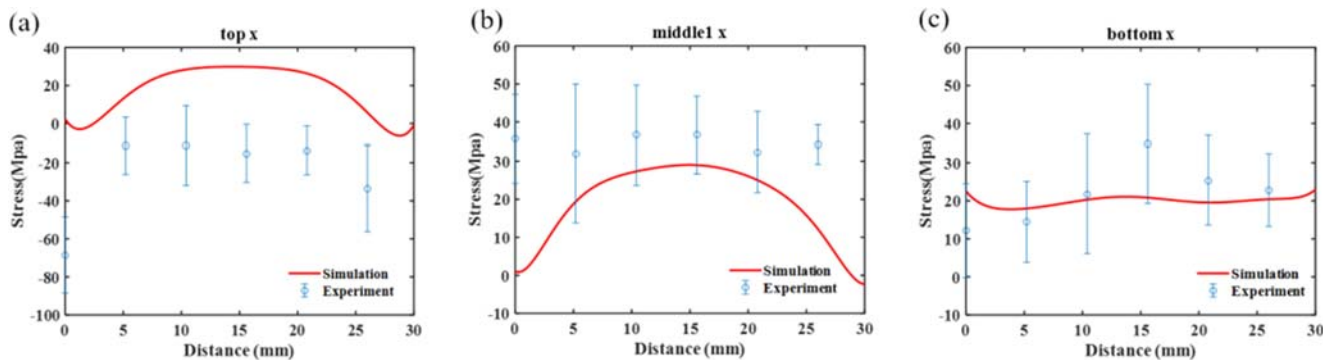
Fig. 6 The residual stress along the midline in the transverse direction. **a** Top layer, **b** middle layer, and **c** bottom layer

[17] is used here to define the material's yield strength with the increase of strain rate. Assuming that the yielding occurs when the stress in the direction of the wave propagation reaches the HEL, the dynamic yield strength under uniaxial strain condition can be defined in terms of the HEL by Braisted and Brockman [18]:

$$\sigma_{dyn} = HEL \frac{1-2v}{1-v} \qquad (11)$$

where v is the Poisson's ratio. In the analysis, the workpiece material is assumed to be homogeneous and isotropic. The plastic strain is assumed to be perfectly elastic-plastic with dynamic yield strength defined as σ_{dyn}, and the basic material properties required for the simulation are shown in Table 2.

The mechanism of stress superposition of LSP on laser additive manufactured sample is plotted in Fig. 4. The stress-strain curve during normal laser peening process can be described as the dashed line in Fig. 4. The σ_L represents the load stress added on the material, and ε_L is the strain on the material, and their relationship can be described as [23]:

$$\sigma_L \begin{cases} \left(K + \frac{4}{3}G\right)\varepsilon_x & \sigma_L \leq \frac{1-v}{1-2v}\sigma_{dyn} \\ K\varepsilon_x + \frac{2}{3}Ys & \sigma_L \geq \frac{1-v}{1-2v}\sigma_{dyn} \end{cases} \qquad (12)$$

where K is the material bulk modulus; G is the material shear modulus; v is the Poisson's ratio; and σ_{dyn} is the dynamic yield strength.

Consider initial stress, define:

$$\sigma_L := \begin{cases} \sigma_{LSP} & \sigma_I = 0 \\ \sigma_I + \sigma_{LSP} & \sigma_I \neq 0 \end{cases} \qquad (13)$$

where σ_{LSP} is the load stress induced by LSP and σ_I represents initial stress. Without initial stress and strain, the LSP-induced stress loading process is plotted as dashed line in Fig. 4. First, the stress rapidly grows up, and elastic deformation occurs. Then, the stress continues to increase and reach the dynamic yield strength limit (point A); the material starts plastic deformation until the load totally attenuates. Finally, the material enters the elastic offload phase, where the elastic deformation release and the plastic deformation remained (point D). When
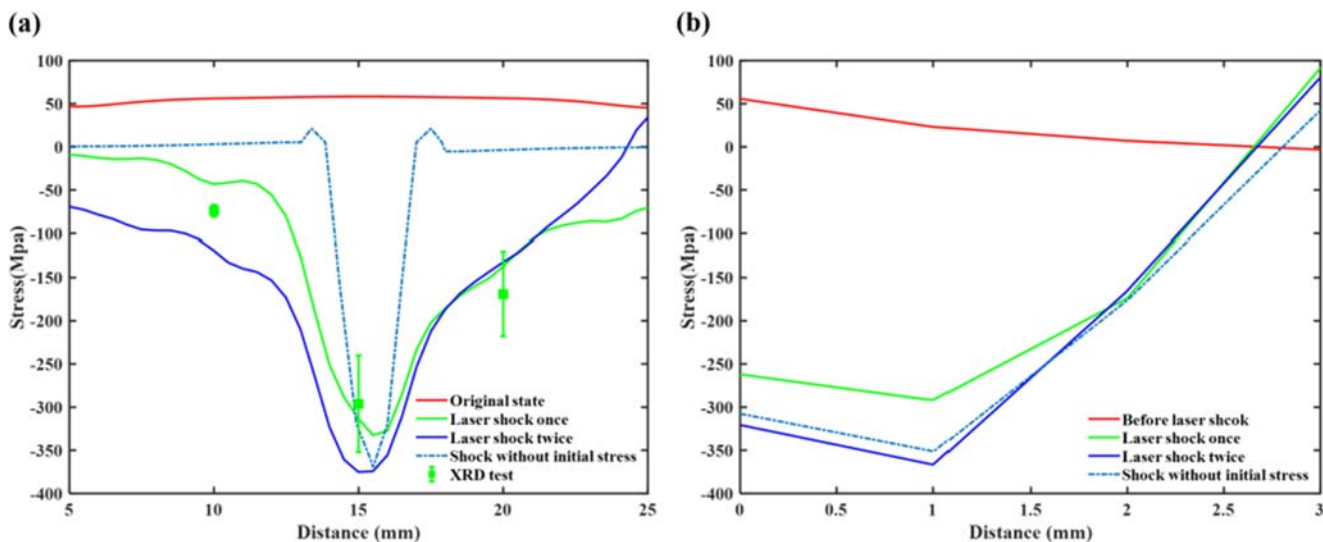

Fig. 7 Residual stress distribution after laser peening. **a** X-direction stress. **b** Stress along the depth
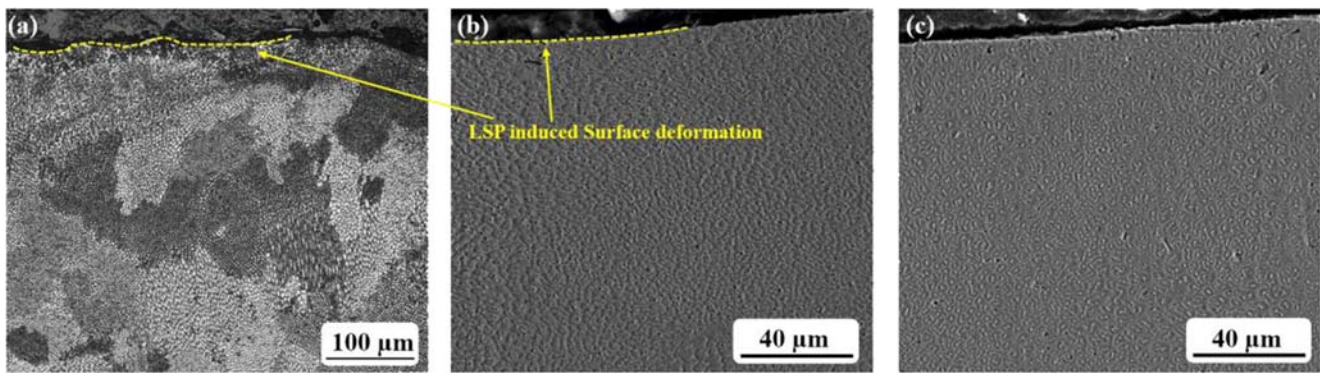
Fig. 8 OM and SEM results. **a** OM result of laser-peened sample. **b** SEM result of laser-deposited sample. **c** SEM result of laser-peened sample

the sample has initial stress which in the same direction as the load stress, the start point of the stress-strain circle moves to point O′, and the load stress σ_L can be written as $\sigma_I + \sigma_{LSP}$. The stress inside of the sample quickly reaches the dynamic limits of the sample. As the increase of the load, additional plastic deformation is created, and the load stage ends at point B′. After offload, the strain remained inside of the sample is a little larger than the normal condition (point D′). Conversely, when the direction of the initial stress is opposite against the load stress, the less plastic strain will remain at the end of the load-offload circle (blue line).

4 Results and discussion

Figure 5 shows the simulated residual stress distribution on the top, middle, and bottom layer of the deposited parts. It is clear to see in all three layers; tensile stress appears in the middle. The stress values on the edge of the sample are lower than those in the center part. A small part of compressive stress appears on the edge of the sample and gradually turns into tensile stress toward the sample center.

To verify the simulation results, the residual stresses are tested along the midline of the sample in the transverse direction (Fig. 2) layer by layer. As plotted in Fig. 6, the trend of the

experiment results and simulation results is barely similar. In the top and middle layers, the stress distribution is like a parabola shape; the tensile stress appears in the center of the sample. While in the bottom layer, the stress curve is relatively flat. The slight mismatch between the experimental and simulation results could be caused by the following reasons: first, due to the manufacturing error, the final shape of the deposited material is hard to be a strictly "cuboid" as modeled in FEM program, and second, the surface quality and grain defects can affect the results of XRD test, while the simulation results are the mean value of the nodes on the observation point.

Figure 7 compares the residual stress distribution before and after LSP process. It is clear to see that before laser peening, the sample surface was occupied with tensile stress, and laser peening successfully imports compressive stress into the sample. It is worth noting that, in laser-deposited sample, a large compressive stress area appears after laser peening. However, in the normal laser peening process, the compressive stress is restricted inside of the laser spot, and few tensile stresses are spotted on the edge of the shocked area (the dot-dash line in Fig. 7a). Figure 7 b plots the stress distribution along the depth direction. When initial stress equals 0, a single shock can create compressive stress as high as − 351.2 MPa. By contrast, with initial tensile stress around 50 MPa, the maximum compressive stress created by single shock is only
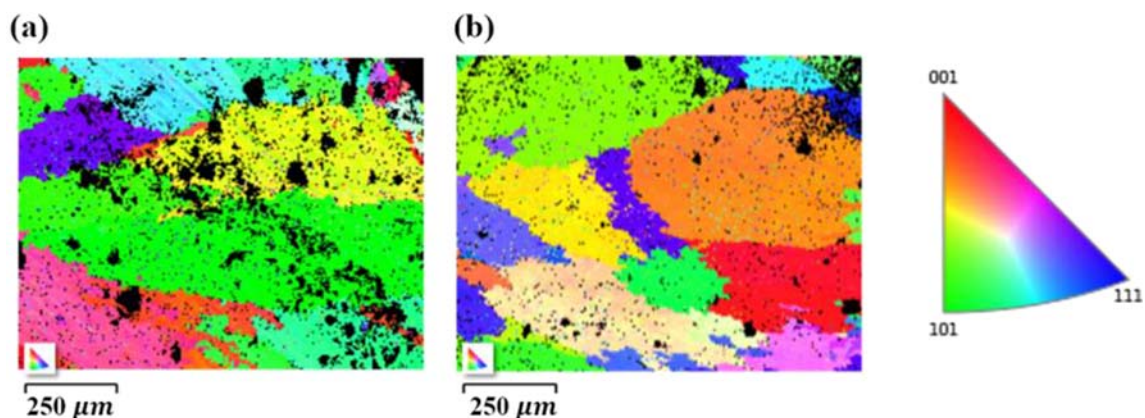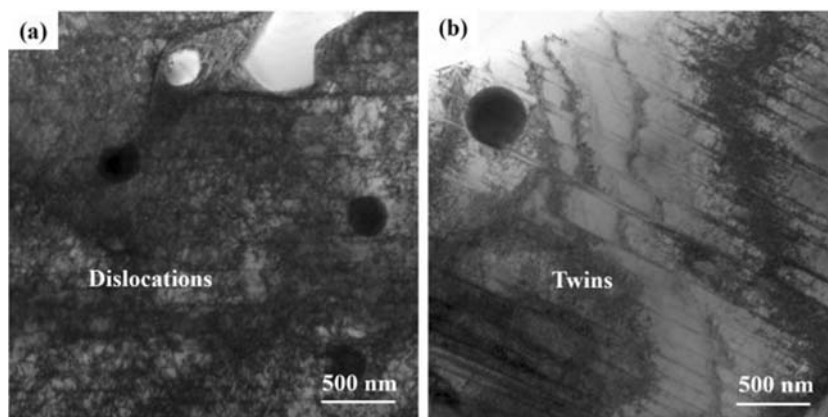

Fig. 9 EBSD results at sample surface. **a** Before laser peening. **b** After laser peening

Fig. 10 The TEM results of laser-peened sample. **a** Laser peening-induced dislocations. **b** Laser peening-induced twins

− 291.6 MPa. It can be also concluded from Fig. 7 a and b; in laser-deposited sample, it costs two shocks to achieve similar value and depth of the compressive residual stress obtained in zero initial stress condition. In Fig. 7 b, the stress curves grow up sharply after 2-mm depth; this reveals the fact that the maximum effective depth of LSP is about 2 mm.

The different results of the residual stress distribution indicate that the internal stress in laser-deposited sample can dramatically influence the laser peeing results. Experienced a repeated heating-cooling cycle during laser deposition process, the contract and expansion of the material created a complex strain and stress field. The residual stresses generated inside the sample are presented as elastic stress. Based on the deformed shape, the stress inside of the sample remains a delicate balance. When an exterior excitation is introduced (e.g., LSP in this work), the stress inside the sample will be redistributed according to the induced strain and generate a coupled residual stress distribution.

Figure 8 a and b are OM and SEM results of LSP-treated sample, and Fig. 8 c is the untreated sample. The microstructure of laser-deposited sample is mainly austenite, and few ferrites are distributed on the grain boundary. Compare the results in Fig. 8 b and c, the microstructure before and after

laser peening looks similar; no distinct phase change is observed after laser peening. To further confirm this result, EBSD analysis was performed on LSPed area. Figure 9 is the EBSD results. It did not show a clear trend of grain refinement after laser peening. Nevertheless, the surface deformation is obvious in both macroscopic and microscopic observations. Usually, the surface deformation induced by conventional surface treatment such as shot peening is accompanied by strain-induced martensitic transformation [24]. However, in this work, no martensitic phase is spotted inside of the sample. Thus, the deformation mechanism of LSP on the laser-deposited sample should be further studied. Figure 10 shows the TEM results of LSPed sample. It can be spotted from Fig. 10 a that a high density of dislocations are formed after laser peening, and the mechanical twins with very thin band are developed. The twins are extremely fine, with thickness in the range from 20 to 40 nm. With such a large amount of microcosmic change inside of the sample, we can deduce that the surface deformation induced by laser peening on laser-deposited sample is the accumulative effects of a massive amount of dislocations and twins. As the laser shock wave propagates along with the depth of the sample, the atoms inside of the sample were pushed forward at a massive speed;
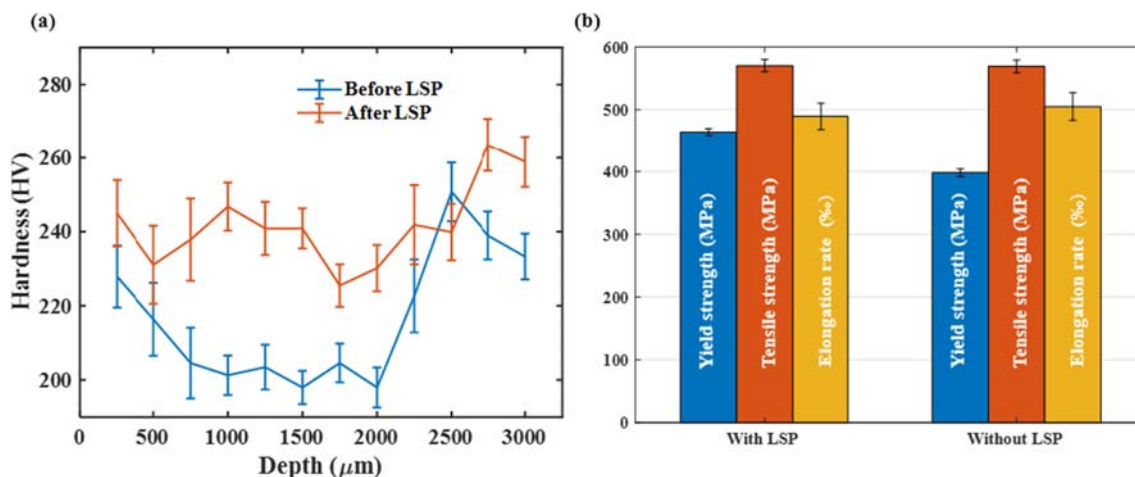

Fig. 11 Mechanical properties of the samples. **a** Microhardness. **b** Tensile test

Table 3 Two sample T test for tensile test results

Index	Sample number	Mean	Standard deviation	Difference	95% CI for difference	P value
Yield strength (MPa) with LSP	6	464.00	5.38	65.97	(58.35, 73.58)	0.000
Yield strength (MPa) without LSP	6	398.03	6.25			
Tensile strength (MPa) with LSP	6	570.30	9.75	1.30	(− 11.69, 14.28)	0.827
Tensile strength (MPa) without LSP	6	569.0	10.1			
Elongation rate (‰) with LSP	6	489.6	21.2	− 15.5	(− 43.8, 12.9)	0.248
Elongation rate (‰) without LSP	6	505.1	22.2			

when the atomic stress exceeds the critical twinning stress of the material, some atoms will move to a new position and change the lattice structure [25]. The lattice structure can be changed and reflected as stack faults and twins. The movement of the atoms also created some non-close-packed atoms and reflected as dislocations. Since the strain rate of laser peening is super high (10^6 s^{-1}), the shock wave did not have enough time to induce a continuous lattice structure change, so the phase transformation is not obvious in our sample.

Figure 11 a depicts the hardness distribution in the depth direction of LSPed and untreated samples. It is clear to see that LSP treatment dramatically improved the hardness of the sample. To verify this deduction, a one-sample T test was performed to determine whether the LSP can enhance the hardness. Before LSP, the samples' mean hardness was 216.7 HV; the result of the T test shows that the confidence interval (CI) of the hardness after LSP is (234.88 HV, 248.91 HV); and the p value equals 0, which means the LSP has significantly improved the hardness of the sample. After LSP, the hardness in the central part increased from 201 to 246 HV, while on the surface, the hardness only increased from 227 to 245 HV. Two facts can affect hardness change. First, the laser-induced high-density dislocations and twins reinforced the mechanical property and increased the surface hardness. Second, the residual stress also contributes to the hardness increment. It can be seen from Fig. 7 b that the laser affected residual stress field reached as depth as 2 mm and the peak value appeared around 1-mm depth which is the center part of the sample. The compressive stress makes the material hard to deform and thus reduced the indented area. Figure 11 b compares the tensile properties of treated and untreated samples (each of the data plotted on the bar chart is the mean value from 6 samples). Combined with the T test results in the Table 3, we can deduce that the LSP has a prominent effect on the yield strength of the material; after LSP the mean value increased from 398 to 464.4 MPa. By contrast, the tensile stress only has a 1.3 MPa increase after treatment. On the other hand, the mean elongation rate of the sample also did not show a remarkable

Fig. 12 Fracture surface morphologies of additive manufactured 316 stainless steel. **a** and **c** Fracture surface micrograph of laser-peened sample. **b** and **d** Fracture surface micrograph of laser-deposited sample (untreated)
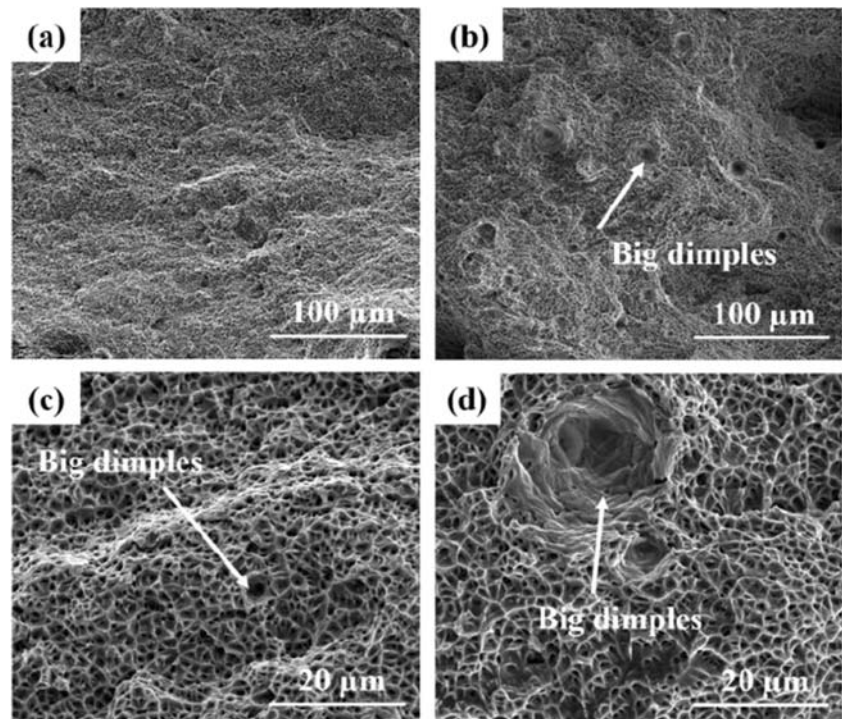
change after LSP; the value only changes 1% after LSP treatment.

Figure 12 compares the fracture morphologies of additive manufactured samples. Figure 12 a and c are laser-peened samples, and Fig. 12 b and d are untreated samples. It can be seen from the pictures that all the samples show a lot of dimples on the fracture surface which means the laser additive manufactured samples have good ductility. Compared with LSPed sample, the dimples in the untreated sample are little coarser than laser-peened sample; although some big dimples are found in the untreated sample, the number of them is small; and combined with *T* test result, we can conclude that the LSP's influence on the ductility is limited.

5 Conclusion

The residual stress, microstructure, and mechanical properties of LSP-treated LAMed 316 steel were studied in this article. The residual stress was studied through a three-dimensional finite element model to reveal the interaction of thermal initial stress and LSP-induced stress. The microstructure and mechanical properties of LSP-treated samples were examined through the experimental method. The main conclusions are as follows:

First, the numerical model built in this article successfully predicted the LSP-induced residual stress on laser additive manufactured sample. The simulations results agreed well with the XRD measured results. The thermal-induced tensile residual stress in laser-deposited sample can affect the laser peening results in both horizontal and longitudinal directions. The tensile initial stress can reduce the compressive stress induced by LSP. In laser-deposited sample, the area of the surface compressive stress induced by LSP was a little larger, but the affected depth is relatively lower when compared with the stress-free sample.

Second, after LSP there is no obvious phase change and grain refinement in OM and SEM and EBSD observation. A large number of dislocations and twins were spotted in TEM results of LSP-treated sample. The LSP-induced surface deformation can be the accumulative effects of the microdisplacement of the atoms driven by LSP-induced shock wave at high strain rate.

Third, some mechanical properties of the LAMed sample were changed after LSP treatment. The hardness on the surface and 1-mm depth have been increased by 7% and 22%, respectively, and the yield strength was increased by 16%, while there is no significant change in the tensile strength and elongation rate.

References

1. Mazumder J, Schifferer A, Choi J (1999) Direct materials deposition: designed macro and microstructure. Mater Res Innov 3:118–131. https://doi.org/10.1007/s100190050137
2. Aqilah DN, Sayuti AKM, Farazila Y et al (2018) Effects of process parameters on the surface roughness of stainless steel 316L parts produced by selective laser melting. J Test Eval 46:20170140. https://doi.org/10.1520/JTE20170140
3. Riza SH, Masood SH (2017) Optimization of process parameters for solid and porous steel alloy structures produced by direct metal deposition. Mater Today Proc 4:8918–8927. https://doi.org/10.1016/j.matpr.2017.07.243
4. Ibarra-Medina J, Pinkerton AJ (2010) A CFD model of the laser, coaxial powder stream and substrate interaction in laser cladding. Phys Procedia 5:337–346. https://doi.org/10.1016/j.phpro.2010.08.060
5. Alberti EA, Bueno BMP, D'Oliveira ASCM (2016) Additive manufacturing using plasma transferred arc. Int J Adv Manuf Technol 83:1861–1871. https://doi.org/10.1007/s00170-015-7697-7
6. Morrow JD, Wang Q, Duffie NA, Pfefferkorn FE (2014) Effects of pulsed laser micro polishing on microstructure and mechanical properties of S7 tool steel. 9th Int Conf MicroManufacturing
7. Kamkarrad H, Narayanswamy S (2016) FEM of residual stress and surface displacement of a single shot in high repetition laser shock peening on biodegradable magnesium implant. J Mech Sci Technol 30:3265–3273. https://doi.org/10.1007/s12206-016-0635-2
8. Fang C, He Y, Lee J-H, Shin K (2016) Effect of ultrasonic shot peening on the microstructural evolution of the 316SS alloy. J Nanosci Nanotechnol 16:11063–11068. https://doi.org/10.1166/jnn.2016.13290
9. Yan X, Wang F, Deng L et al (2018) Effect of laser shock peening on the microstructures and properties of oxide-dispersion-strengthened austenitic steels. Adv Eng Mater 20:1–8. https://doi.org/10.1002/adem.201700641
10. Kalentics N, Huang K, Ortega Varela de Seijas M, et al (2019) Laser shock peening: a promising tool for tailoring metallic microstructures in selective laser melting. J Mater Process Technol 266:612–618. https://doi.org/10.1016/j.jmatprotec.2018.11.024
11. Kalentics N, Boillat E, Peyre P et al (2017) Tailoring residual stress profile of selective laser melted parts by laser shock peening. Addit Manuf 16:90–97. https://doi.org/10.1016/j.addma.2017.05.008
12. Hackel L, Rankin JR, Rubenchik A et al (2018) Laser peening: a tool for additive manufacturing post-processing. Addit Manuf 24:67–75. https://doi.org/10.1016/j.addma.2018.09.013
13. Martinez Hurtado A, Francis JA, Stevens NPC (2016) An assessment of residual stress mitigation strategies for laser clad deposits. Mater Sci Technol 32:1484–1494. https://doi.org/10.1080/02670836.2016.1192766
14. Guo W, Sun R, Song B et al (2018) Laser shock peening of laser additive manufactured Ti6Al4V titanium alloy. Surf Coatings Technol 349:503–510. https://doi.org/10.1016/j.surfcoat.2018.06.020
15. Sun R, Li L, Zhu Y et al (2018) Microstructure, residual stress and tensile properties control of wire-arc additive manufactured 2319 aluminum alloy with laser shock peening. J Alloys Compd 747:255–265. https://doi.org/10.1016/j.jallcom.2018.02.353
16. Shiva S, Palani IA, Paul CP, Singh B (2018) Comparative investigation on the effects of laser annealing and laser shock peening on

the as-manufactured Ni–Ti shape memory alloy structures developed by laser additive manufacturing. Pp 1–20

17. Kalentics N, Boillat E, Peyre P et al (2017) Materials & design 3D laser shock peening – a new method for the 3D control of residual stresses in selective laser melting. Mater Des 130:350–356. https://doi.org/10.1016/j.matdes.2017.05.083

18. Toyserkani E, Khajepour A, Corbin S (2004) 3-D finite element modeling of laser cladding by powder injection: effects of laser pulse shaping on the process. Opt Lasers Eng 41:849–867. https://doi.org/10.1016/S0143-8166(03)00063-0

19. Heigel JC, Michaleris P, Reutzel EW (2015) Thermo-mechanical model development and validation of directed energy deposition additive manufacturing of Ti-6Al-4V. Addit Manuf 5:9–19. https://doi.org/10.1016/j.addma.2014.10.003

20. Mills KC (2002) Fe - 316 stainless steel. In: Recommended values of thermophysical properties for selected commercial alloys. Woodhead Publishing, p Pages 135–142,

21. Hussein A, Hao L, Yan C, Everson R (2013) Finite element simulation of the temperature and stress fields in single layers built without-support in selective laser melting. Mater Des 52:638–647. https://doi.org/10.1016/j.matdes.2013.05.070

22. Malik A, Manna A (2019) Application of lasers in manufacturing. Springer Singapore

23. Wang L (2005) Foundation of shock waves. National Defense Industry Press

24. Altenberger I, Scholtes B, Martin U, Oettel H (1999) Cyclic deformation and near surface microstructures of shot peened or deep rolled austenitic stainless steel AISI 304. 264:1–16

25. Luo SN, An Q, Germann TC, Han LB (2009) Shock-induced spall in solid and liquid Cu at extreme strain rates. J Appl Phys:106. https://doi.org/10.1063/1.3158062